Correspondence to:

L. Chutia and J. Wang,
lakhima-chutia@uiowa.edu;
jun-wang-1@uiowa.edu

Author Contributions:

Conceptualization: Lakhima Chutia, Jun Wang
Data curation: Lakhima Chutia, Xi Chen, Zhendong Lu, Meng Zhou
Formal analysis: Lakhima Chutia
Funding acquisition: Jun Wang
Investigation: Lakhima Chutia
Methodology: Lakhima Chutia, Jun Wang
Project administration: Jun Wang, Eric M. Wilcox
Software: Lakhima Chutia
Supervision: Jun Wang, Eric M. Wilcox
Validation: Lakhima Chutia

Correlated Modes of Spatiotemporal Variations Between Biomass Burning Aerosols and Tropospheric Temperature Over the Indian Region

Lakhima Chutia[1,2] [ORCID], **Jun Wang[1,2]** [ORCID], **Xi Chen[1,2]**, **Zhendong Lu[1,2]** [ORCID], **Meng Zhou[1,2]**, and **Eric M. Wilcox[3]** [ORCID]

[1]Department of Chemical and Biochemical Engineering, University of Iowa, Iowa, IA, USA, [2]Center for Global and Regional Environmental Research, University of Iowa, Iowa, IA, USA, [3]Division of Atmospheric Sciences, Desert Research Institute, Reno, NV, USA

Abstract Biomass burning aerosols influence atmospheric temperatures by absorbing solar radiation, thereby altering the contrast between day and night temperatures. This study investigates the correlation between these aerosols and day-night (D-N) temperature changes over India by applying principal component analysis (PCA) in long-term (2003–2021) satellite observations (MODIS AOD, AIRS D-N temperature at 850 hPa, MOPITT CO) and MERRA-2 reanalysis data. Mode analysis for the premonsoon period identifies biomass burning in northeast India as the dominant source of the second mode of AOD, BC AOD, and CO, with strong covariations between BC AOD and AOD ($R = 0.90$) and between CO and AOD ($R > 0.79$). PCA of satellite observations shows that long-term variation of AOD and D-N temperature at 850 hPa in the second mode is strongly correlated ($R = 0.83$), highlighting the sensitivity of diurnal temperature variations to light-absorbing aerosols. This strong relationship is further confirmed with MERRA-2 reanalysis data. Moreover, high correlations ($R > 0.85$) between BC AOD and D-N temperature in the second mode validate the role of biomass burning in driving long-term diurnal temperature contrast. Reconstruction analysis over northeast India indicates that the BC AOD fraction accounts for approximately 42% of the D-N temperature variability during the 19-year study period. These findings not only quantify the critical role of biomass burning aerosols in modulating diurnal temperature variations across the Indian region but also provide satellite observation-based insights that have the potential to constrain the aerosol radiative effects on the atmospheric temperature profile in climate models.

Plain Language Summary Biomass burning from slash-and-burn agriculture and crop residue burning releases small heat-absorbing particles into the atmosphere. These particles, especially black carbon, are highly effective at absorbing sunlight and warming the air, which can lead to changes in day and night temperature patterns. In this study, we used 19 years of satellite and reanalysis data to explore the relationship between these particles and the difference between daytime and nighttime temperatures over India. We found that during the premonsoon season, biomass burning in northeast India, particularly from traditional farming practices like shifting cultivation, has a strong link with day-night temperature patterns. In fact, the fraction of black carbon in total aerosol optical depth explained a considerable portion (~42%) of the variation of lower-atmospheric temperatures between day and night. This study provides firsthand evidence by combining long-term satellite and model data to study the relationship between burning-dominated particles and day-night temperature differences in India and to quantify their impact from climate point of view.

1. Introduction

Light-absorbing aerosols originating from both natural and anthropogenic sources, such as black carbon (BC), brown carbon, and mineral dust, exert a significant influence on the three-dimensional distribution of atmospheric temperature by absorbing solar radiation, resulting in substantial atmospheric heating and surface cooling (Davidi et al., 2009, 2012; Li et al., 2022; Wang & Christopher, 2006; Zhang et al., 2020). This influence is particularly pronounced in regions with high aerosol concentrations, such as the Indian subcontinent, where biomass burning, dust, and anthropogenic emissions are significant contributors to the overall aerosol loading (Jethva et al., 2019; Pan et al., 2015; Sarkar et al., 2019). BC aerosol dominates (≥75%) the aerosol absorption in this region (Ramachandran et al., 2020), leading to high atmospheric heating rates of about 1.9–2.0 K Day^{-1}, notably in the megacity Delhi, primarily attributed to agricultural burning effects (Bisht et al., 2015). Recent observations

Visualization: Lakhima Chutia
Writing – original draft: Lakhima Chutia
Writing – review & editing:
Lakhima Chutia, Jun Wang, Xi Chen,
Zhendong Lu, Meng Zhou, Eric M. Wilcox

further indicate aerosol-induced atmospheric heating rates of 0.48–0.72 K Day^{-1} over the Indo-Gangetic Plain, with aerosols accounting for more than 50% of the total warming of lower atmosphere in this region (Ramachandran et al., 2023). However, their association with the tropospheric day-night (D-N) temperature contrast, defined as the difference between daytime and nighttime tropospheric temperatures, remains unexplored.

The northeastern part of India, particularly during the premonsoon season, experiences widespread biomass burning activity associated with slash-and-burn agricultural practices, which leads to seasonally elevated concentrations of absorbing aerosols such as black carbon. Borgohain et al. (2023) reported that fire activity peaks in March and April in this region, with an average of 65,000 fire counts and surface BC concentrations reaching up to 3.15 µg m^{-3}. Similarly, Badarinath et al. (2009) and Gogoi et al. (2017) showed that biomass burning during the premonsoon period enhances aerosol loading and contributes to atmospheric warming in northeast India. These studies provide a strong basis for examining the relationship between aerosols and temperature in this region during the premonsoon season. In this context, the present study focuses primarily on biomass burning aerosols, which make a substantial contribution to the light-absorbing aerosol loading and radiative effects over northeast India during the premonsoon period. Given the complex topography and persistent, widespread biomass burning activity, a comprehensive approach integrating both long-term observation-based and modeling approaches is essential to fully understand the signature of tropospheric diurnal temperature change induced by these aerosols in this region.

Analyzing the day and night temperature change with aerosol optical depth (AOD) in climatological studies can elucidate how biomass burning and other light-absorbing aerosols contribute to excess daytime heating compared to nighttime. Unraveling this relationship will enable us to better understand the complex interaction between aerosols and temperature dynamics throughout the day. If based on observational data, these insights could help constrain the representation of absorbing aerosol heating and its vertical distribution in climate models, which remain major sources of uncertainty in simulated aerosol radiative forcing (Myhre et al., 2013; Samset et al., 2018). Previous studies have explored changes in atmospheric temperature profiles due to smoke loading over various regions, particularly over oceanic areas such as the Amazon basin (Davidi et al., 2009) and offshore southern Africa (Wilcox, 2010), as well as land regions like the Yucatan Peninsula and southern Mexico (Wang & Christopher, 2006). More recently, studies over the Indian region reported that summertime surface temperature maxima in northwest India correlate with the abundance of absorbing aerosols (Dave et al., 2020). Bharali et al. (2019) revealed significant cooling within the boundary layer and slight warming above 1 km due to absorbing aerosols during daytime over the Indo-Gangetic Plain. Additionally, weak correlations between diurnal temperature changes (Tmax–Tmin) and variations in the BC burden have been observed in India and China across winter and summer seasons through climate model simulations (Stjern et al., 2020). However, none of these studies have explored the long-term mode variability between tropospheric D-N temperature contrast and biomass burning-driven light-absorbing aerosols using either modeling or observational data, indicating a significant gap in the literature regarding the aerosol radiative feedback on the diurnal variation of temperature and meteorological parameters, such as temperature itself, on both global and regional scales.

This study presents a unique approach to address this significant gap in existing literature. First, we aim to unravel the relationship between mode variations of light-absorbing aerosols, primarily those associated with biomass burning and D-N temperature contrast, which, to the best of our knowledge, has not been explored before over the Indian region. Second, we adopt an integrated approach, utilizing long-term data sets from both modeling and observational sources, to provide a comprehensive analysis on this subject. Third, we employ the principal component analysis (PCA) method (details in Section 2) to examine the correlated mode variability between temperature contrast and absorbing aerosols, as well as key spatiotemporal patterns of temperature change attributing to the aerosol radiative feedback. Due to the orthogonality between different modes in PCA, this approach is useful to identify the fingerprints (e.g., spatiotemporal variations) of aerosols on temperature without detailed treatment of other confounding factors (e.g., variation of daily weather and meteorological regimes). Unlike conventional correlation analysis, PCA reduces dimensionality and filters out short-term fluctuations, allowing a mode-based interpretation of spatiotemporal covariability between aerosols and temperature in noisy, heterogeneous data sets, especially in regions with diverse aerosol sources and complex terrain, such as India.

A 19-year record (2003–2021) of satellite and reanalysis data in the 21st century is used to study the link between major modes of variability in 3D distributions of aerosols and D-N temperature contrast over the Indian region,

with particular emphasis on northeast India, where biomass burning is pronounced during the premonsoon season. These major modes of variability, derived from PCA, represent a statistically robust approach, previously employed to reveal dominant global aerosol patterns by Li et al. (2013) and to analyze land surface temperature variability by Song et al. (2021). To our knowledge, this study is the first attempt of using PCA to unravel the interconnected variation of biomass burning-driven light-absorbing aerosols and D-N temperature contrast. Additionally, carbon monoxide (CO) data are used as a proxy to further aid, evaluate, and interpret the analysis of the dominant mode of absorbing aerosols because CO and light-absorbing fine-mode aerosols (smoke, BC) often have similar sources with incomplete combustion.

Section 2 describes the methodology employed in this study. Section 3 introduces the data sets used, including AOD from Modern-Era Retrospective analysis for Research and Applications version 2 (MERRA-2) and Moderate Resolution Imaging Spectroradiometer (MODIS) Level 3 products; day and nighttime temperature from MERRA-2 and the Atmospheric Infrared Sounder (AIRS); CO column data from Measurements of Pollution in the Troposphere (MOPITT) and MERRA-2; and speciated AOD data from MERRA-2, including black carbon AOD (BC AOD), organic carbon AOD (OC AOD), and sulfate AOD. Section 4 presents our findings, starting from the mode analysis of absorbing aerosols (Section 4.1) and D-N temperature and its attribution (Section 4.2), followed by the mode analysis for reconstructed data (Section 4.3). The discussion and conclusions are provided in Sections 5 and 6.

2. Methodology

The principal component analysis (PCA) for the aforementioned data sets in 2003–2021 is performed to explore the correlated variations of biomass burning-driven light-absorbing aerosols and tropospheric temperature over the Indian region. PCA, first introduced by Pearson (1901), is a statistical approach that employs orthogonal transformations to create a new set of independent variables, called the principal components, which capture the essential information of the original data, with 1st component explaining the highest variability, the 2nd component explaining the second most variability, and so on (Hotelling, 1933; Jolliffe, 2002). PCA is widely applied in climate and environmental studies to identify the dominant modes in spatiotemporal variations of variables such as sea and land surface temperature, AOD, dust particles, etc. (Li et al., 2013; Lu et al., 2023; Song et al., 2021; Khoir et al., 2022). This approach is particularly useful for unraveling aerosol-temperature relationships in regions with diverse aerosol sources and complex terrain, such as over India.

If we consider a data matrix X of size N x M, where N is the number of locations and M is the number of observations, then the PCA is calculated by computing the eigenvectors of the covariance matrix C (Li et al., 2013)

$$C = \frac{1}{M-1} X X^T \tag{1}$$

C is an $N \times N$ real, positive semidefinite matrix and can thus be expressed as follows:

$$C = E \Lambda E^T \tag{2}$$

Where E is an orthogonal matrix comprising the N orthogonal eigenvectors, often referred to as empirical orthogonal functions (EOFs) and Λ represents a diagonal matrix containing the N eigenvalues of C. The principal components (PCs) are determined by projecting the data matrix on the corresponding EOF and can be computed as

$$P = X^T E \tag{3}$$

Matrix P has a dimension of $M \times N$, whose columns represent the N principal components; thus, P and E satisfy

$$X = E P^T \tag{4}$$

Combining equations Equations 1, 2, and 4, we can write the diagonal matrix Λ as

$$\Lambda = \frac{1}{M-1} P \, P^T \tag{5}$$

The principal components are mutually orthogonal, and the eigenvalues of Λ represent their variances.

Before conducting the analysis, we preprocessed the data by removing the mean of each column of the data matrix. We used monthly data covering the premonsoon months (March, April, and May) for each year from 2003 to 2021, with each month treated as an independent sample in the PCA, which allows us to focus on spatio-temporal variability across seasonal observations.

In this study, PCA was applied separately to each data set (e.g., MODIS AOD, AIRS D-N temperature, MOPITT CO, and MERRA-2 aerosol and temperature variables). To ensure consistency across data sets, we used monthly Level 3 gridded satellite products (MODIS, AIRS, and MOPITT) at $1° \times 1°$ resolution. MERRA-2 variables were used at their original $0.5° \times 0.625°$ resolution. Each data set was processed independently to identify dominant spatial modes and their associated temporal variability using PCA. We then examined the temporal covariability between principal components representing biomass burning related aerosol variability and those representing temperature variability. In addition, MERRA-2 aerosol and temperature fields were reconstructed from the selected principal mode to assess spatiotemporal correlations in the biomass burning-dominated region.

3. Data Sets

3.1. MODerate Resolution Imaging Spectroradiometer (MODIS)

MODIS instruments onboard NASA's Terra (since 1999) and Aqua (since 2002) satellites have been providing continuous aerosol measurements for over 20 years. It acquires data in 36 spectral channels with wavelengths ranging from 0.4 to 14.4 μm and spatial resolutions varying from 250 m to 1 km, achieving complete global coverage every 1–2 days (Levy et al., 2007). Two operational algorithms, Dark Target (DT) and Deep Blue (DB), are employed for retrieving AOD from MODIS, with comprehensive descriptions available in prior studies (Levy et al., 2013a; Remer et al., 2005). Extensive validation of MODIS AOD has been conducted globally and regionally, establishing its credibility and widespread utilization in aerosol and climate studies (Gupta et al., 2018; Ma et al., 2016; Payra et al., 2023; Wei et al., 2019). For this study, we utilized gridded monthly Level 3 MODIS Aqua (MYD08_M3) combined Dark Target and Deep Blue AOD product at 1° spatial resolution (Platnick et al., 2015) over the Indian region during the period 2003–2021.

3.2. Atmospheric Infrared Sounder (AIRS)

The Atmospheric Infrared Sounder (AIRS) onboard NASA's EOS Aqua satellite is a grating spectrometer with 2378 infrared channels and four visible/near-infrared channels, providing 3D measurements of temperature, water vapor, and other earth/atmospheric products throughout the atmospheric column (CHAHINE et al., 2006). The swath width of AIRS is 1,650 km with a horizontal resolution of 13.5 and 2.3 km at the nadir for infrared and visible/near-infrared channels, respectively (Aumann et al., 2003). Here, we have utilized AIRS L3 Monthly Standard Physical Retrieval (AIRS-only) $1° \times 1°$ V7.0 (AIRS3STM v7.0) daytime and nighttime air temperature data at 850 hPa for the period 2003–2021. Level 3 air temperature products are gridded averages of the AIRS L2 air temperature onto $1° \times 1°$ latitude/longitude grid cells, covering pressure levels from 1,000 to 1 hPa, and are reported separately for ascending and descending orbits (Tian et al., 2020). The D-N temperature contrast in this study is computed by subtracting the temperature in the descending (nighttime, 01:30 LT) mode from the ascending (daytime, 13:30 LT) mode. Details regarding the L3 version 7 products, retrieval algorithm, and validation can be found in various studies (Ding et al., 2020; Zhang et al., 2023).

As AIRS retrieves temperatures at fixed local times, the computed D-N temperature contrast may underestimate the full diurnal temperature range. However, our study focuses on long-term spatiotemporal variability instead of capturing the full diurnal amplitude. The consistent twice-daily sampling from AIRS provides a reliable basis for comparing relative variations in D-N temperature contrast across regions and over time (Ruzmaikin et al., 2017). Therefore, long-term AIRS observations remain suitable for analyzing D-N temperature contrast to investigate aerosol-temperature covariability.

Here, we selected daytime and nighttime temperature data at 850 hPa (∼1,500 m) for this study. In regions where biomass burning is prevalent during the premonsoon season, such as northeast India, terrain elevations generally remain below 1,500 m (see Figure S1a in Supporting Information S1), making 850 hPa suitable for representing free-tropospheric conditions while reducing the influence of surface heterogeneity and topographic effects on temperature retrieval. Moreover, vertical profile analysis (Figure S1b in Supporting Information S1) shows that the D-N temperature difference peaks around 850–925 hPa. Since 925 hPa can fall below the surface in elevated areas, 850 hPa provides a more reliable and consistent level. Additionally, we found that the correlation between MERRA-2 BC AOD and D-N temperature is strongest at 850 hPa (figure not shown), indicating that this level best captures the thermal response to absorbing aerosols. These findings are consistent with previous studies that reported enhanced aerosol-induced heating at altitudes of around 1–2 km (e.g., Kant et al., 2023).

### 3.3. Measurements Of Pollution In The Troposphere (MOPITT)

The Level 3 monthly column CO data at 1° × 1° latitude-longitude grid was obtained from Measurements Of Pollution In The Troposphere (MOPITT) version 8 (MOP03T_8) for the period 2003–2021. MOPITT, onboard NASA's EOS Terra satellite, is a nadir-viewing gas correlation radiometer providing measurements of CO in different layers of the troposphere since March 2000 on a global scale (Deeter, Edwards, Francis, Gille, Mao, et al., 2019; Drummond, 1993). It measures upwelling radiation in both thermal infrared (TIR; 4.7 μm) and near-infrared (NIR; 2.3 μm) bands (Drummond et al., 2022). MOPITT's spatial resolution is 22 km at nadir, with a swath width of 640 km, equator crossing at 10:30/22:30 local time, and global coverage every 3 days. A detailed description of the measurement technique and the retrieval algorithm can be found in various studies (e.g., Deeter et al., 2003). The MOPITT CO data have been widely used for various applications such as long-term trend analyses, interannual variability assessments, exploration of emission sources, and CO budget construction (Girach & Nair, 2014; Strode & Pawson, 2013; Zhang et al., 2020). Extensive evaluations of MOPITT's performance have been documented on both global and regional scales, including assessments over the Indian region (Buchholz et al., 2017; Deeter et al., 2017; Emmons et al., 2009).

3.4. MERRA-2 Reanalysis

We also utilized the Modern-Era Retrospective analysis for Research and Applications version-2 (MERRA-2) monthly data, including AOD and its speciation (BC AOD, OC AOD, AAOD, and sulfate AOD), column CO, and day and night temperature at 850 hPa from 2003 to 2021 over the Indian region. These column-integrated aerosol variables are widely used in climatological studies to represent regional aerosol burden and radiative effects. MERRA-2, a global reanalysis data set from NASA's Global Modeling and Assimilation Office (GMAO), encompasses earth observations since 1980, assimilating meteorological data and AODs from various ground- and satellite-based sources (Gelaro et al., 2017; Randles et al., 2017). It utilizes the upgraded version (Version 5.12.4) of the Goddard Earth Observing System Model, version 5 (GEOS-5) data assimilation system (Rienecker et al., 2008) and provides meteorological and chemical fields at a resolution of 0.625° × 0.5° with 72 hybrid-eta levels from the surface to 0.01 hPa. MERRA-2 assimilates bias-corrected AOD from MODIS, AVHRR, and MISR (over bright surfaces), as well as from AERONET. It employs the Goddard Chemistry, Aerosol, Radiation, and Transport (GOCART) aerosol module to simulate externally mixed aerosol mass mixing ratio tracers, including dust, sea salt, BC, organic carbon, and sulfate (Randles et al., 2017). Anthropogenic BC, sulfate, and primary organic matter (POM) emissions are obtained from AEROsol COMparisons between Observations and Models (AeroCom) Phase II (Diehl et al., 2012), with further details provided in Randles et al. (2017). MOPITT CO is not assimilated in MERRA-2. MERRA-2 has been shown to reasonably capture aerosol distributions over India (e.g., Buchard et al., 2017; Kuttippurath & Raj, 2021; Pandey & Vinoj, 2021). A detailed description of the MERRA-2 input observation system and validation of meteorological and chemical fields are available in several previous studies (Bosilovich et al., 2015; McCarty et al., 2016).

4. Results

The distribution of AOD across the Indian region is significantly influenced by the prevalence of distinct aerosol types that vary throughout the seasons (see Figures 1a–1d). While multiple sources, including dust, vehicular, industrial, and residential emissions, contribute to aerosols across India, their relative influence varies regionally and seasonally. During the premonsoon season (March–May), higher AOD is observed over northeast India, primarily due to biomass burning emissions related to shifting or jhum cultivation practices (Figures 1a and 1e).
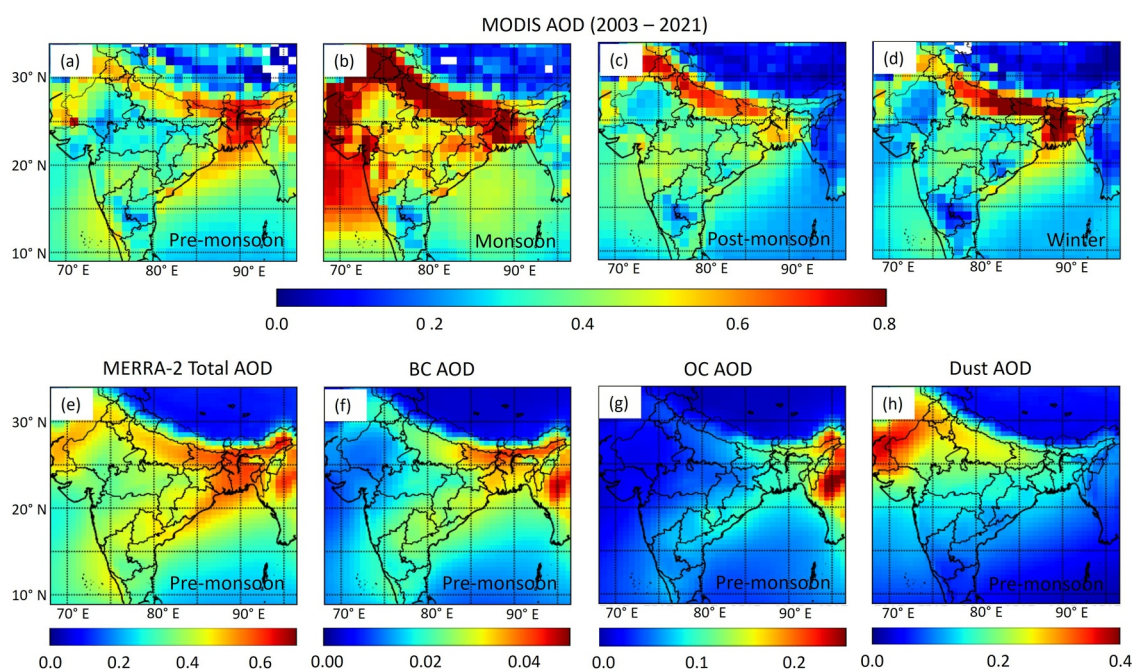
Figure 1. Seasonal distribution of MODIS AOD over the Indian region from 2003 to 2021 (panels a–d), along with the spatial distributions of (e) total AOD, (f) black carbon (BC), (g) organic carbon (OC), and (h) dust AOD from MERRA-2 reanalysis during the premonsoon period of 2003–2021.

MODIS daily fire detections (blue line) and their 30-day rolling mean (orange line) consistently peak between March and May each year, further supporting the seasonal dominance and persistence of biomass burning in northeast India (see Figure S2 in Supporting Information S1). Previous studies (e.g., Badarinath et al., 2009; Borgohain et al., 2023; Gogoi et al., 2017) have also identified biomass burning as a key contributor to aerosol loading in this region and season. This region exhibits high concentrations of carbonaceous aerosols, particularly BC and OC AOD (Figures 1f and 1g), while dust AOD is largely confined to western India (Figure 1h). In contrast, biomass burning in northwest India and anthropogenic emissions, mostly over the densely populated Indo-Gangetic Plain, play a dominant role in the postmonsoon (September–November) and winter (December–February) seasons (Figures 1c and 1d). Similarly, BC AOD, the key light-absorbing aerosol, also shows a distinct seasonal pattern (See Figure S3 in Supporting Information S1). In the premonsoon season, BC is emitted mainly from biomass burning in northeast India, while in the postmonsoon and winter season, it shows a more mixed composition of biomass burning and anthropogenic emissions from highly populated areas (Figure S3 in Supporting Information S1; David et al., 2018).

Given the clearer dominance of biomass burning during the premonsoon season, we conducted PCA specifically for this period to investigate the correlation between light-absorbing aerosols and D-N temperature over this region during 2003–2021. Focusing on the premonsoon period allows for a more robust analysis than other seasons, where aerosol sources are more complex and entangled. Additionally, we did not include dust aerosols in the PCA analysis, as their contribution is spatially limited to western India during the premonsoon season (see Figure 1h) and does not significantly overlap with the biomass burning-dominated region of northeast India. To identify the dominant patterns of variability in aerosol and D-N temperature, we first applied PCA over the entire Indian region for the premonsoon season. This broader spatial domain allowed us to separate region-specific aerosol modes. We then focused the reconstruction analysis over northeast India, where biomass burning aerosols are prevalent, to quantify their contribution to the D-N temperature contrast.

### 4.1. Mode Analysis of Light-Absorbing Aerosols

To understand the spatiotemporal variability of light-absorbing aerosols and their relationship to D-N temperature contrast, we first applied PCA to satellite and reanalysis AOD data sets. The main goal of this analysis is to identify the dominant patterns in aerosol loading, particularly those associated with biomass burning, and to
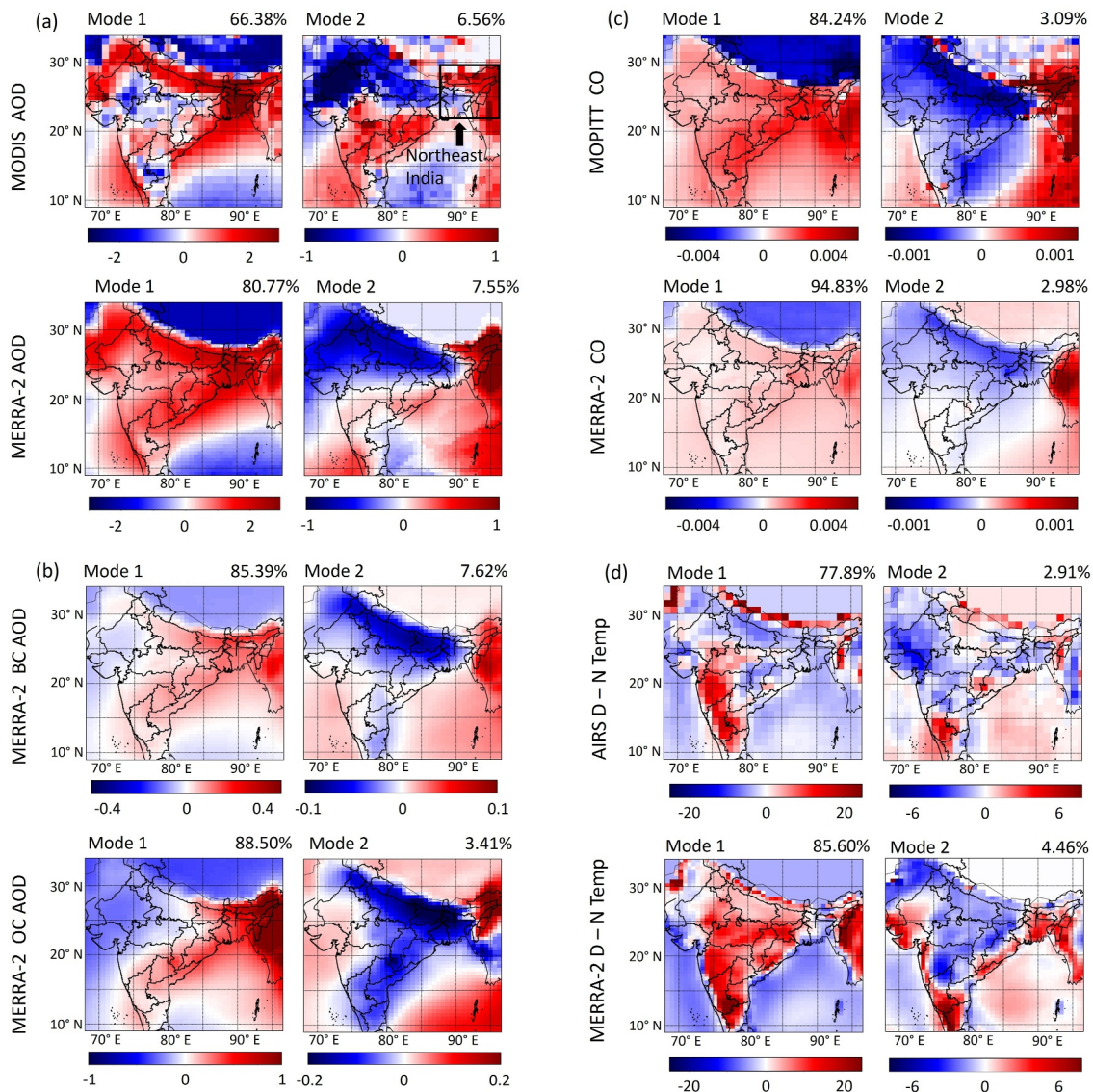
Figure 2. The first two modes of PCA analysis for (a) MODIS and MERRA-2 AOD, (b) MERRA-2 BC and OC AOD, (c) MOPITT and MERRA-2 CO column, and (d) AIRS and MERRA-2 D-N temperature data during premonsoon months (Mar–Apr–May) of 2003–2021 over the Indian region. The variance of each mode is shown as a percentage at the top of each panel. The color scales indicate the sign and magnitude of the EOF loadings, with red indicating positive values and blue indicating negative values.

distinguish them from other aerosol sources such as dust and anthropogenic emissions. This approach allows us to isolate the modes dominated by biomass burning for further evaluation and attribution to the D-N temperature contrast, particularly during the premonsoon season.

As described in Section 2, each PCA mode consists of a spatial pattern (EOF) and a corresponding time series (PC). The spatial variability of MODIS and MERRA-2 AOD data over the Indian region during the premonsoon period is predominantly explained by the first four PCA modes, accounting for 80%–93% of the total variance (Figure 2a and Figure S4a in Supporting Information S1). Specifically, the first two modes together explain 73% and 88% of the variance in MODIS and MERRA-2 data, respectively (Figure 2a). The spatial patterns corresponding to these modes exhibit strong agreement between MODIS and MERRA-2 AOD (Figure 2a). In the PCA maps (Figure 2), the red and blue color gradients represent the sign and magnitude of the EOF loadings, with red indicating positive loadings and blue indicating negative ones. When the associated PC value is positive, AOD increases in regions with positive loadings (red areas) and decreases in regions with negative loadings (blue areas)
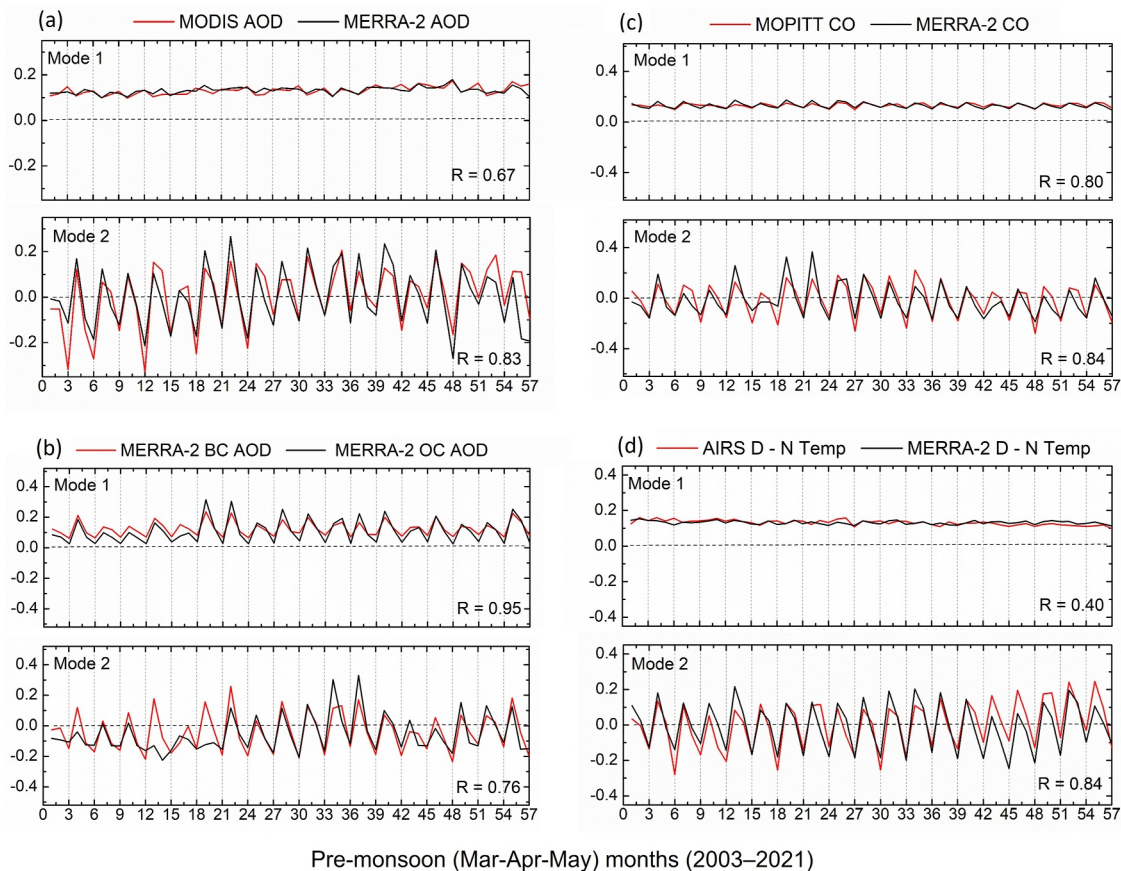
Figure 3. The PC time series of the first two modes for (a) MODIS and MERRA-2 AOD, (b) MERRA-2 BC and OC AOD, (c) MOPITT and MERRA-2 CO column, and (d) AIRS and MERRA-2 D-N temperature data during premonsoon months (Mar–Apr–May) of 2003–2021 over the Indian region. Each point along the *x*-axis represents an individual premonsoon month (March, April, and May) from 2003 to 2021. The *y*-axis represents the PC time series values (unitless). The data are treated as independent observations in the PCA.

and vice versa when the PC value is negative. This approach enables us to identify distinct aerosol patterns and their associated temporal variability. Modes 3 and 4 contribute minimally to the overall variance, accounting for ~2%–4% in MODIS and 1%–2% in MERRA-2 data (see Figure S4a in Supporting Information S1). Therefore, we will focus our discussion only on the first two modes. Quantitatively, MODIS shows greater variability than MERRA-2 in the first two modes (Figure 2a), which is consistent with previous studies, indicating higher variability in MODIS data than other satellites (e.g., OMI and MISR) over regions, especially over the Thar desert and the Indo-Gangetic Plain (Li et al., 2014). Mode 1 represents a mixture of biomass burning and dust aerosols (Figure 2a). The westerly wind transports mineral dust from arid regions and the Thar desert in western India, carrying it into the Indo-Gangetic Plain and northern India (Figure 1h; Kumar et al., 2015). Mode 2 is predominantly attributed to biomass burning activities in northeast India, especially from slash-and-burn agriculture practices such as jhum or shifting cultivation (Figure 2a second column; Figure S2 in Supporting Information S1). This mode highlights the presence of absorbing aerosols like BC and OC (see Figures 1f and 1g for the spatial distribution of BC and OC AOD). To examine the temporal evolution of these modes, we analyzed the associated PC time series shown in Figure 3a for the first two modes and in Figure S5a of Supporting Information S1 for modes 3 and 4. There is a weak and consistent seasonal cycle in the first mode for both MODIS and MERRA-2 data (with a linear correlation coefficient *R* of 0.67), suggesting a stable mean state of emissions (Figure 3a top panel). In contrast, significant variability is evident in the second mode (bottom panel in Figure 3a), reflecting year-to-year changes in biomass burning emissions during the premonsoon season. This large temporal variability is reflected in both MODIS and MERRA-2 data sets, with a correlation coefficient of 0.83 (bottom panel in Figure 3a). The assimilation of bias-corrected AOD from MODIS into the MERRA-2 reanalysis enhances the consistency between the data sets.
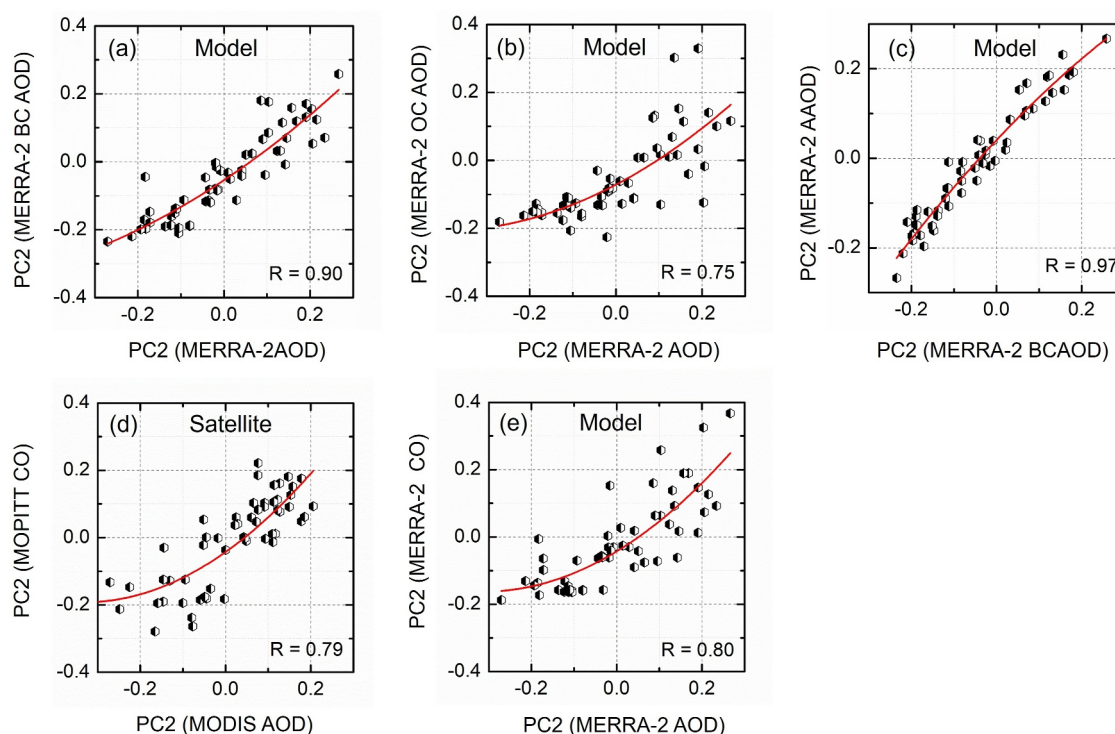
Figure 4. Scatterplots showing (a and b) the relationship between PC2 BC AOD and PC2 OC AOD with PC2 AOD from MERRA-2, (c) the relationship between PC2 BC AOD and PC2 AAOD from MERRA-2, (d) the relationship between PC2 AOD from MODIS and PC2 CO from MOPITT, and (e) same as figure (d) but using MERRA-2 AOD and CO data during the premonsoon period (2003–2021).

Since MERRA-2 closely resembles satellite observations, we extended our analysis using MERRA-2 data to perform PCA on carbonaceous AOD (BC and OC AOD) over the Indian region (Figure 2b and Figure S4b in Supporting Information S1). The first two modes together explain approximately 92% of the total variance (Figure 2b). Mode 1 primarily reflects large-scale background variability in carbonaceous aerosols, whereas Mode 2 highlights the influence of biomass burning, particularly over northeast India. Strong correlations between BC and OC time series in both modes ($R = 0.95$ for Mode 1 and $R = 0.76$ for Mode 2, Figure 3b) indicate overall covariability of these species. However, the biomass burning signal is especially evident in Mode 2, where the principal components of BC and OC AOD show strong covariation with Mode 2 AOD, with correlation coefficients of 0.90 between BC AOD and AOD and 0.75 between OC AOD and AOD (Figures 4a and 4b). Additionally, the combined contributions of PC2 BC and OC AOD show a strong correlation ($R = 0.88$) with PC2 AOD, further supporting these findings (Figure S6a in Supporting Information S1). This analysis indicates that biomass burning is the driving factor of AOD variance, primarily through the contributions of both BC and OC.

To further investigate the dominant modes of absorbing aerosols, we expanded our PCA analysis for CO, a tracer for biomass burning with similar sources to light-absorbing aerosols. Similar to AOD, BC, and OC AOD, modes 3 and 4 of CO account for only a small fraction (0.41%–1.21%) of the total variance (Figure S4c in Supporting Information S1). The first mode of the MOPITT CO column reflects a combination of anthropogenic and biomass burning sources, explaining 84% of the total variance, with a very weak cycle evident in the time series plots (top panels in Figures 2c and 3c, respectively). Mode 2 is predominantly influenced by biomass burning in northeast India, explaining 3% of the total variance (Figure 2c). Similarly, the PCA modes from MERRA-2 resemble those of MOPITT CO, accounting for 97% of the variance; however, MOPITT shows greater variability across all modes (Figure 2c). Both data sets indicate significant loading of biomass burning emissions from northeast India, with a strong correlation of 0.84 between their Mode 2 time series (Figure 3c). Both the PC2 of MOPITT and MERRA-2 CO exhibit strong correlations with the PC2 of AOD, with coefficients of 0.79 for satellite data and 0.80 for model data, reflecting their common biomass burning sources (Figures 4d and 4e).

To validate that the aerosols associated with Mode 2 are both biomass burning in origin and strongly absorbing in nature, we extended our PCA analysis to include MERRA-2—absorbing aerosol optical depth (AAOD) and the AAOD/AOD fraction, which provide direct proxies for aerosol radiative absorption. The second PCA modes of both AAOD and AAOD/AOD closely resemble the spatial and temporal patterns of BC AOD and CO, with particularly strong loadings over northeast India (Figures S7a and S7b in Supporting Information S1). The second principal component of AAOD shows a strong correlation with that of BC AOD ($R = 0.97$), highlighting that BC AOD is a strong indicator of absorbing aerosol variability during the premonsoon season in this region (Figure 4c).

Overall, this analysis shows that the second PCA mode across multiple aerosol indicators, including AOD, BC AOD, OC AOD, CO, and AAOD, captures a strong biomass burning signal over northeast India during the premonsoon season. The consistent spatial and temporal patterns across these variables confirm that Mode 2 is dominated by biomass burning related emissions. Moreover, the inclusion of AAOD and the AAOD/AOD fraction highlights that BC AOD is a reliable proxy for absorbing aerosols. In the following section, we examine how these absorbing aerosols covary with D-N temperature contrast during the premonsoon season.

4.2. Mode Analysis of Temperature and Its Attribution

The first two PCA modes of AIRS and MERRA-2 D-N temperature at 850 hPa, along with their corresponding time series during the premonsoon months, are presented in Figures 2d and 3d. Together, these modes account for 81% and 90% of the total variance in AIRS and MERRA-2 data, respectively. Mode 1 appears to be driven by topography (Figure 2d) and shows a weak cycle (Figure 3d), whereas Mode 2 exhibits significant variability with a strong correlation ($R = 0.84$) between the AIRS and MERRA-2 time series (Figures 2d and 3d). In Mode 2 (Figure 2d, right column), northeast India shows positive loadings (red), indicating that when the PC time series (Figure 3d) is positive, the D-N temperature contrast tends to be stronger in this region and weaker when the PC values are negative. Contributions from Modes 3 and 4 are minimal (1%–2%), as indicated in Figure S4d of Supporting Information S1. Therefore, we selected the Mode 2 D-N temperature, which best captures interannual changes in temperature contrast during the premonsoon season, to further investigate the link between D-N temperature variations and absorbing aerosols.

We conducted correlation analysis between the D-N temperature difference associated with the second principal component (PC2) and the PC2 of biomass burning-dominated aerosol variables, as identified in Section 4.1, including PC2 of AOD, BC AOD, OC AOD, and CO (Figure 5). A significant correlation is observed between PC2 of AOD from MODIS and PC2 of D-N temperature from AIRS, with a correlation coefficient of 0.83 (Figure 5a). Similarly, the correlation between PC2 of MERRA-2 absorbing AOD and PC2 of D-N temperature is 0.84 (Figure 5b). These strong correlations from both the model and satellite data highlight the sensitivity of D-N temperature differences to variations in light-absorbing aerosols and their interconnection via radiative feedback processes. Larger temperature differences correspond to higher amounts of absorbing aerosols, implying that these aerosols contribute to excess daytime heating. The strong agreement between satellite observations and reanalysis data strengthens our findings, emphasizing the reliability of the relationship between absorbing aerosols and D-N temperature contrast across different data sets.

Given the strong association between the second principal components of AOD and CO (Figures 4d and 4e), we next analyze how the PC2 of the CO column, dominated by biomass burning, correlates with the PC2 of D-N temperature difference (Figures 5c and 5d). We observe that CO exhibits a strong correlation ($R > 0.81$) with D-N temperature differences in PC2 in both satellite and reanalysis data (Figures 5c and 5d). This finding supports our hypothesis that the PC2 of AOD, which shows a strong covariation with the PC2 of CO, is dominated by absorbing aerosols and is positively correlated with D-N temperature variations. Furthermore, high correlations are observed between the PC2 of AAOD and the AAOD/AOD ratio with the PC2 of D-N temperature contrast ($R = 0.90$ and 0.93, Figures S7c and S7d in Supporting Information S1), highlighting the important contribution of absorbing aerosols to the D-N temperature contrast. Additional analysis, presented in Figures 5e and 5f, reveals a strong association ($R = 0.72$–0.89) between the PC2 of both biomass burning-dominated BC and OC AOD and the PC2 of D-N temperature, further emphasizing their impact on D-N temperature variations. Moreover, the combined BC and OC AOD in PC2 shows a strong relationship ($R = 0.86$) with the PC2 of temperature contrast, supporting our hypothesis (Figure S6b in Supporting Information S1).
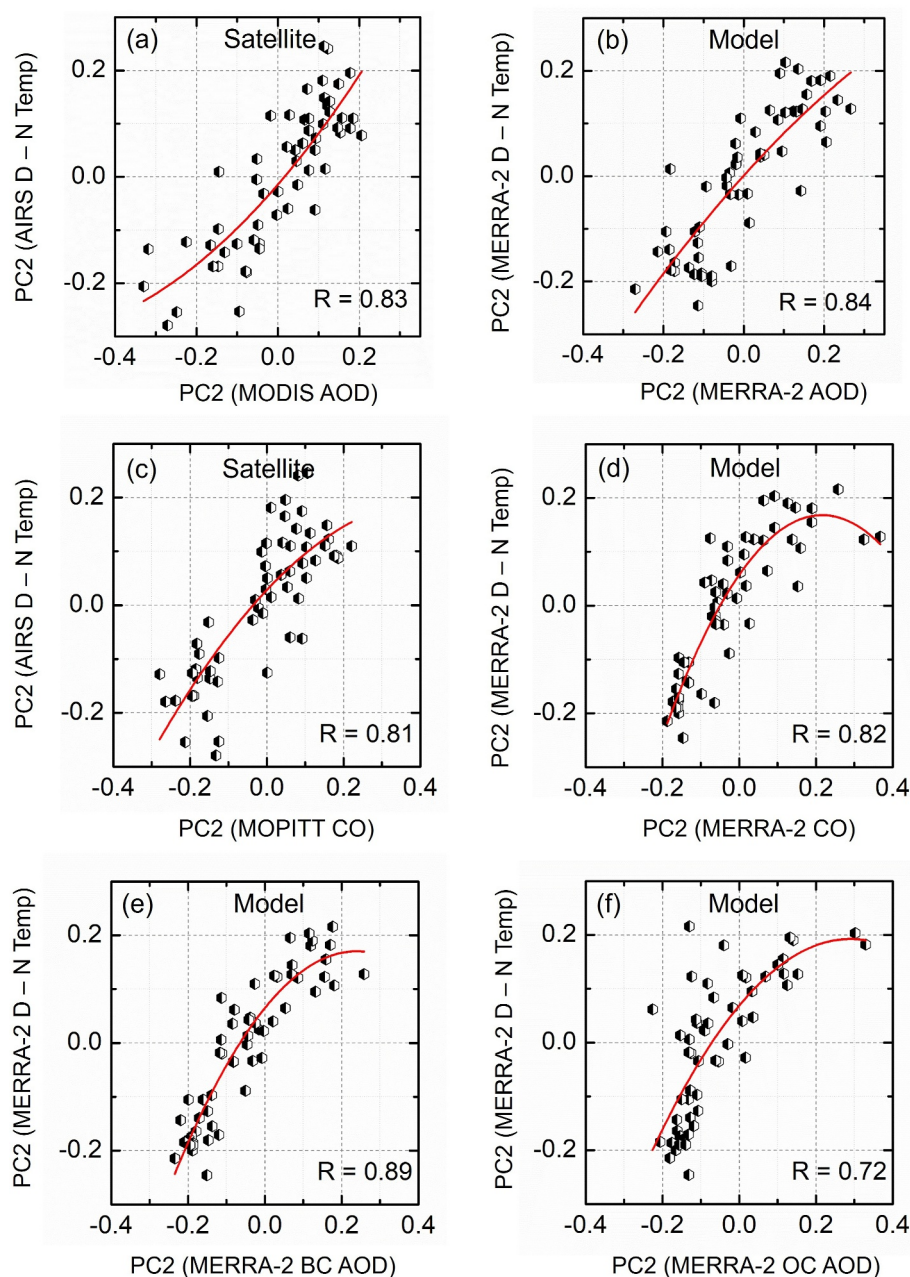
Figure 5. Scatterplots illustrating various relationships during the premonsoon period of 2003–2021: (a) Relationship between PC2 AOD from MODIS and PC2 D-N temperature from AIRS. (b) Same as (a) but with MERRA-2 AOD and temperature data. (c) Relationship between PC2 CO from MOPITT and PC2 D-N temperature from AIRS. (d) Same as (c) but using MERRA-2 CO and temperature data. (e and f) Relationship between PC2 BC and OC AOD with PC2 D-N temperature form MERRA-2.

4.3. Analysis of Reconstructed Data

To further quantify the relationship between absorbing aerosols and D-N temperature variations, we reconstructed AOD, BC AOD, and D-N temperature data using Mode 2 from MERRA-2 reanalysis. Because of the orthogonality and linearity of the different modes in PCA, the reconstruction of the data by modes allows us to reveal the mode-based relationship among multiple variables in their original physical space. Since the fraction of BC AOD regulates aerosol single scattering albedo, that in turn affects the effectiveness of solar absorption (per unit of AOD), we utilized Mode 1 to reconstruct the BC AOD fraction, which represents the relative contribution of BC
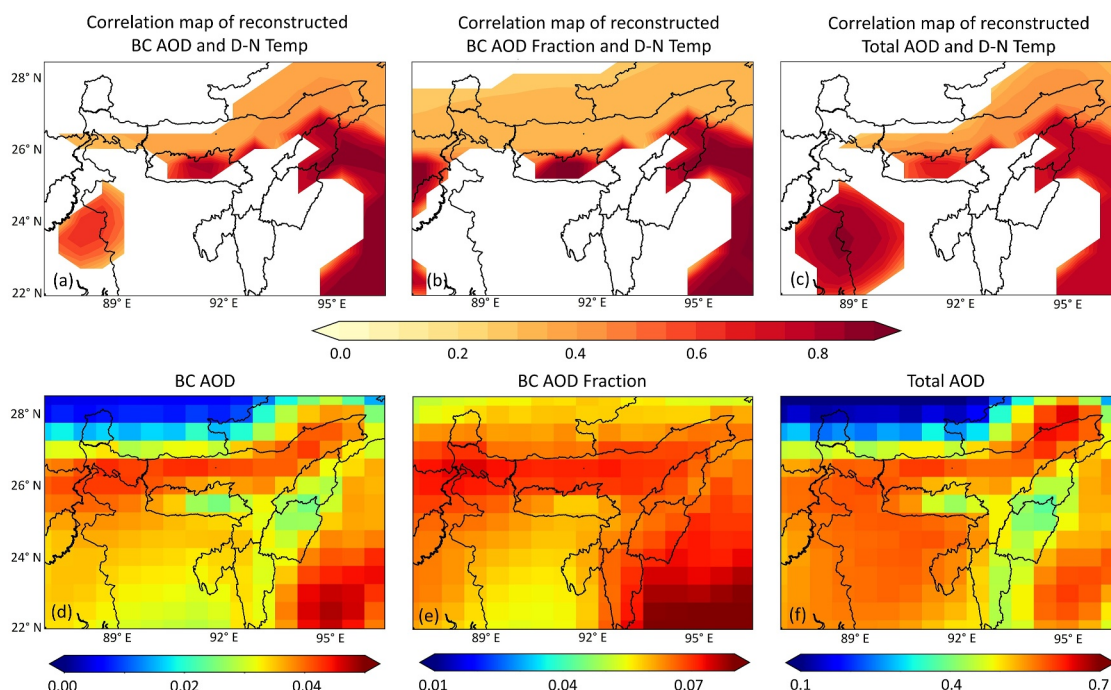
Figure 6. Correlation maps showing the relationship between reconstructed (a) BC AOD and D-N temperature, (b) BC AOD fraction and D-N temperature, and (c) total AOD and D-N temperature from MERRA-2 over northeast India during the premonsoon period (2003–2021). BC AOD, total AOD, and D-N temperature are reconstructed using Mode 2, while BC AOD fraction is reconstructed using Mode 1. Regions where correlations are not statistically significant ($p < 0.05$) and where the annual average BC AOD is below 0.03, BC AOD fraction is below 0.05 and total AOD below 0.2 are masked out. Panels (d), (e), and (f) show the spatial distribution of BC AOD, BC AOD fraction, and total AOD, respectively, over northeast India during the same period.

to the total aerosol loading (Figure S8a in Supporting Information S1). This mode closely resembles the spatial pattern of the BC AOD fraction (Figure 6e), highlighting the significant influence of biomass burning in northeastern India, and exhibits a strong correlation ($R = 0.91$) with D-N temperature variations, as depicted in Figure S8b of Supporting Information S1. By focusing on the modes that are predominantly influenced by biomass burning aerosols, this reconstruction enables us to isolate the impact of absorbing AOD on the spatial and temporal distributions of D-N temperature contrast while minimizing interference from other aerosol sources.

A statistically significant correlation analysis was conducted over northeastern India, where biomass burning is particularly prevalent during the premonsoon season (Figures 6a–6c). We masked out regions where the annual average BC AOD fraction and BC AOD were below 0.05 and 0.03, respectively. The reconstruction revealed a significant positive correlation ($R = 0.20$–0.88) in the upper part of northeastern India between BC AOD, BC AOD fraction, and D-N temperature contrast at 850 hPa, indicating that higher BC levels correspond to greater D-N temperature differences (Figures 6a and 6b). This finding is further supported by the spatial distribution of BC AOD and its fraction, which show higher values in the upper northeastern region, where absorbing aerosols are largely driven by biomass burning (Figures 6d and 6e). Significant positive correlations with D-N temperature contrast are observed in those areas where both BC AOD and its fraction show higher values (Figures 6a and 6b).

Similarly, total AOD and D-N temperature contrast also show significant positive correlations in this region (Figure 6c), emphasizing that the overall aerosol burden contributes to enhanced diurnal temperature variations. In contrast, the lower part of northeastern India and Bangladesh displays higher sulfate AOD and its fraction, indicating the prevalence of scattering aerosols (Figures S9a and S9b in Supporting Information S1). The correlation between BC AOD and D-N temperature contrast is largely insignificant in regions where sulfate aerosols dominate, and a negative correlation is observed between the sulfate AOD fraction and the D-N temperature contrast in those areas (Figure S9c in Supporting Information S1). Notably, the similar patterns observed for both BC AOD and the BC fraction of total AOD versus D-N temperature contrast highlight the important role of absorbing aerosols in increasing daytime heating more than nighttime cooling, resulting in a larger diurnal temperature range. This effect is consistent with previous studies (e.g., Wang & Christopher, 2006; Wilcox

et al., 2016), which showed that smoke absorption significantly increases atmospheric heating due to reduced turbulent mixing and surface influence. By isolating the dominant PCA modes associated with biomass burning aerosols, our reconstruction highlights the statistically significant covariability between absorbing aerosol loading and D-N temperature contrast during the premonsoon season over northeast India. Nevertheless, other contributing factors, such as cloud cover, which reduces daytime maximum temperature and suppresses the diurnal temperature range (Dai et al., 1999); land surface properties, including soil moisture and vegetation cover, which alter the surface energy balance (Shen et al., 2017); and boundary layer dynamics, which regulate nighttime cooling efficiency (Acevedo & Fitzjarrald, 2001), can also influence D-N temperature variability. Such processes may modulate or interact with aerosol-radiation effects and contribute to the overall temperature dynamics. Our focus here, however, is to demonstrate that changes in D-N temperature patterns can, in part, be statistically explained by the spatial and temporal distributions of light-absorbing aerosols.
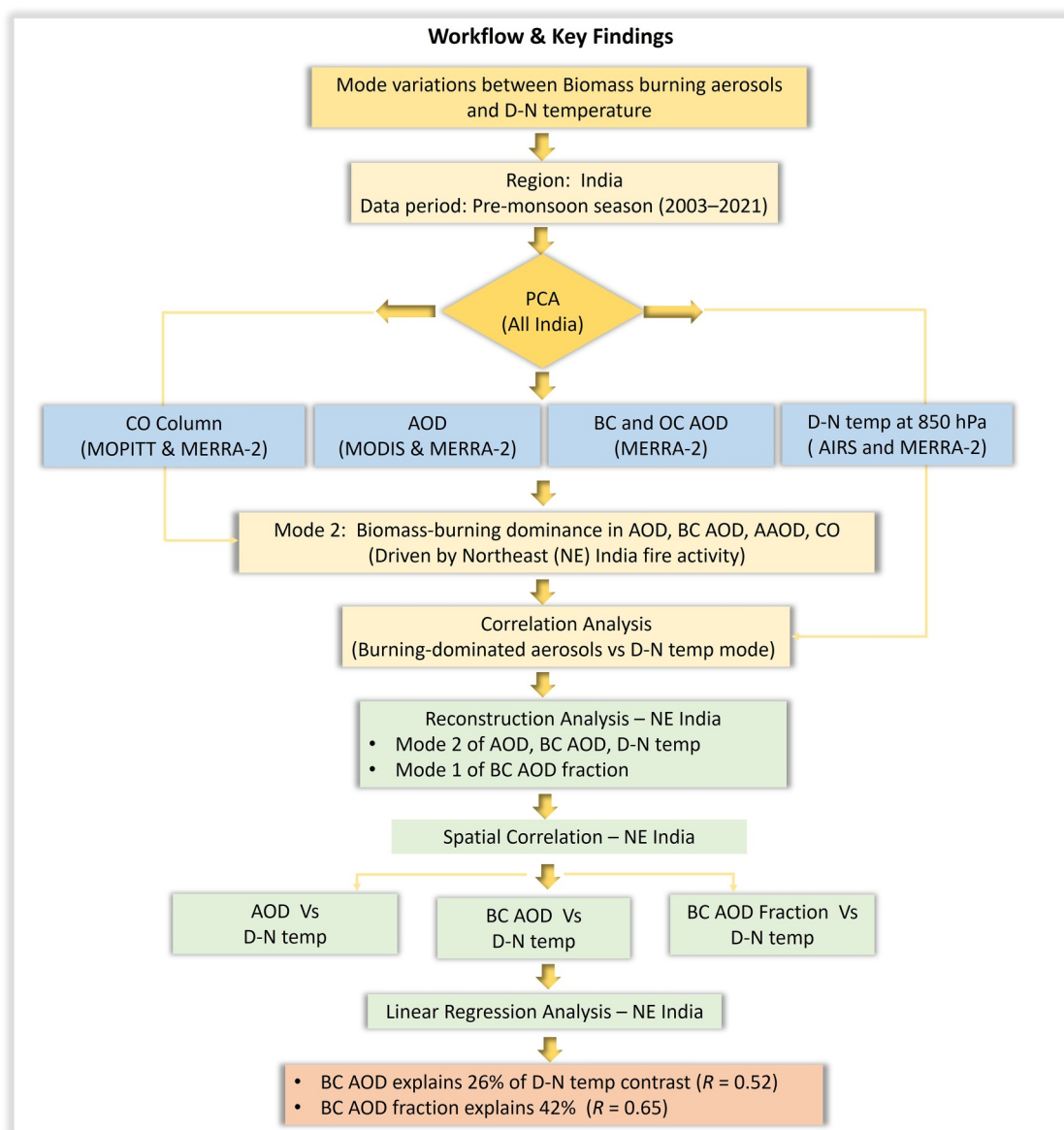
5. Discussion

Figure 7 provides an overview of the workflow and key findings of the study, illustrating the data sets, statistical analyses (PCA, correlation, reconstruction, and regression), and the stepwise progression from analyses over the entire Indian region to northeast India specific analyses. Our findings highlight the important role of biomass burning aerosols in regulating D-N temperature contrast, particularly during the premonsoon season when emissions from biomass burning in northeast India are most intense. During this period, slash-and-burn agricultural farming methods like jhum or shifting cultivation in northeast India significantly contribute to aerosol loading in this region.

Previous studies by Mondal et al. (2021) investigated the impact of absorbing aerosols on summertime surface temperature maxima, particularly in northwest India; however, their influence on D-N temperature variations over the Indian region has not been investigated. Our findings provide new insights into this relationship by revealing a significant positive correlation between absorbing AOD and D-N temperature contrast, particularly over regions where biomass burning is prevalent. The reconstruction analysis indicates that absorbing aerosols contribute to enhanced daytime warming due to increased solar radiation absorption, which leads to boundary layer stabilization and reduced turbulent mixing. At night, the absence of solar radiation and the limited interaction of absorbing aerosols with longwave radiation significantly reduce their radiative heating effect, resulting in weaker nighttime warming, thereby increasing the diurnal temperature range. These mechanisms align with previous model-based research demonstrating that aerosol-induced radiative effects can modify temperature profiles (Ramanathan et al., 2007). However, our study provides an observational constraint on this relationship, highlighting the need for more accurate integration of aerosol-induced warming effects in climate models.

To quantify the contribution of absorbing aerosols to D-N temperature variations, we examined the percentage of D-N temperature variability explained by BC AOD and the BC AOD fraction (Figure 8). Our results show that BC AOD accounts for 27% of the variability in D-N temperature contrast, with a correlation coefficient of 0.52, while the BC fraction of total AOD explains nearly 42% of the variability, with a stronger correlation coefficient of 0.65 (Figures 8a and 8b). This implies that the BC fraction of AOD is a more effective indicator than BC AOD itself in representing the heating effect of absorbing aerosols. The BC fraction represents the relative dominance of light-absorbing particles within the total aerosol burden, essentially capturing the aerosol absorption efficiency and the balance between light-absorbing and scattering aerosols that governs atmospheric heating and, consequently, the D-N temperature contrast (Ramachandran & Kedia, 2010). In contrast, BC AOD represents the column-integrated optical depth attributable specifically to BC particles, indicating their overall atmospheric burden and contribution to solar radiation absorption. Additionally, linear regression analysis shows that especially in regions where biomass burning emissions are prevalent, small changes in BC AOD and its fraction can have a substantial impact on the D-N temperature contrast, further emphasizing the important role of aerosol absorption in regulating D-N temperature patterns. The remaining unexplained variability may be contributed by other meteorological and surface processes, such as cloud cover, land surface properties, boundary layer dynamics, and scattering aerosols that primarily reflect solar radiation and induce surface cooling, all of which can affect the diurnal temperature cycle (Acevedo & Fitzjarrald, 2001; Dai et al., 1999; Shen et al., 2017).

To the best of our knowledge, this is the first study to employ a multiyear data set of D-N temperature alongside AOD, using PCA to assess the relationship between absorbing aerosols and D-N temperature contrast over India. By combining both satellite observations and reanalysis data sets, our study presents a more observationally

Figure 7. Workflow and key findings of the study, showing the data sets, statistical analyses (PCA, correlation, reconstruction, and regression), and the stepwise progression from analyses over the entire Indian region to northeast India-specific analyses. Color coding indicates yellow/orange for all-India PCA steps/results, green for northeast India-specific steps/results, blue for data sets, and brown for key quantitative results.

constrained assessment of the spatiotemporal variability of light-absorbing aerosols and D-N temperature contrast. Our analysis over a 19-year record provides direct observational evidence that biomass burning aerosols, particularly black carbon, play a vital role in regulating D-N temperature variations over northeastern India. This contribution is further supported by the significant fraction of D-N temperature variability explained by the BC fraction of total AOD. The 850 hPa temperature level (~1.5 km) is physically meaningful for this analysis, as it lies within the lower troposphere where most biomass burning aerosols are concentrated. Over India, BC concentrations have been shown to decrease with altitude, with the majority confined below ~3 km (e.g., Kant et al., 2023; Safai et al., 2012). While our analysis uses column-integrated aerosol properties such as AOD, AAOD, and BC AOD, the spatial pattern of BC concentrations at 850 hPa closely resembles that of column-integrated BC AOD and shows strong correlation ($R = 0.87$) with D-N temperature contrast, supporting the vertical representativeness of our approach (see Figure S10 in Supporting Information S1). Although uncertainties in MERRA-2 may influence the absolute magnitude, their overall influence on our results is likely minimal. Our analysis is based on long-term
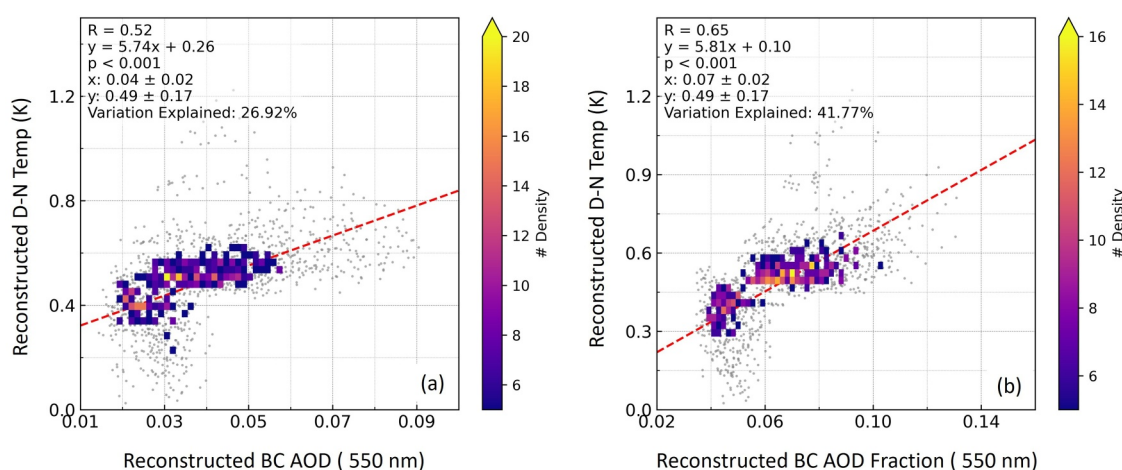
Figure 8. (a and b). Scatterplots illustrating the relationship between reconstructed BC AOD (Mode 2) and the BC AOD fraction (Mode 1) versus D-N temperature (Mode 2) from MERRA-2 data over northeast India during the premonsoon period (2003–2021). The plots display the Pearson correlation coefficient (R), the percentage of variance explained, and the mean ± standard deviation for both axes. Gray dots represent data at each spatial grid point from the 19-year MERRA-2 record, while the overlaid colored shading indicates the density of data points within each bin, highlighting regions of higher data density.

monthly climatology and focuses on dominant mode patterns, which help minimize sensitivity to short-term fluctuations. Furthermore, the consistent patterns observed across satellite observations and reanalysis data sets strengthen confidence in the aerosol-temperature relationship identified in this study.

Overall, our analysis provides important evidence that absorbing aerosols, particularly those from biomass burning, play a key role in modulating the D-N temperature contrast over northeast India during the premonsoon period. By applying the well-established PCA approach that filters out short-term fluctuations, we are able to assess, from a statistical perspective, whether long-term satellite and reanalysis data reveal a detectable impact of light-absorbing aerosols on D-N temperature. These findings also provide important insights that have the potential to better constrain aerosol radiative effects on atmospheric temperature profiles in climate models. We emphasize, however, that the results represent a statistically significant covariability between biomass burning aerosol indicators and D-N temperature contrast during the premonsoon season in this region, rather than a comprehensive source attribution for the entire Indian region. Other physical factors, such as land-atmosphere interactions, boundary layer processes, and cloud cover, may also influence this variability and should be considered in future observational and modeling studies.

6. Conclusions

The study investigated the correlated variability between light-absorbing aerosols and D-N temperature variations over India, with a particular focus on the premonsoon season over northeast India, by employing PCA on long-term satellite and reanalysis data for the period 2003–2021. Our analysis revealed that during the premonsoon season, biomass burning in northeastern India is the major contributor to Mode 2 AOD, along with BC AOD and CO. The second mode of D-N temperature contrast shows significant variability and exhibits a strong correlation ($R > 0.83$) with the second principal component of biomass burning-dominated AOD and BC AOD. The consistency between satellite observations and reanalysis data strengthens our findings, highlighting the associated spatiotemporal variability between burning-dominated aerosols and D-N temperature contrast across multiple data sets. The mode reconstruction analysis further verifies this relationship and reveals a significant positive correlation between absorbing AOD and D-N temperature contrast, suggesting that higher levels of absorbing aerosols are associated with greater D-N temperature differences. Linear regression analysis shows that BC AOD explains 27% of the variability in D-N temperature contrast ($R = 0.52$), while the BC fraction of total AOD accounts for 42% ($R = 0.65$) in the 19-year long-term data record over northeast India.

This study provides firsthand information on the relationship between mode variations of light-absorbing aerosols and D-N temperature variations over India by applying PCA to a multiyear data set combining both satellite and reanalysis data. Our findings highlight the important role of biomass burning aerosols, particularly BC, in modulating regional temperature dynamics. The results reveal statistically significant covariability between

biomass burning aerosol indicators and D-N temperature contrast during the premonsoon season over northeast India, indicating that part of the observed variability in D-N temperature can be statistically detected and explained by the spatial and temporal distributions of these aerosols. By applying the well-established PCA approach that reduces dimensionality and filters out short-term fluctuations, this study not only quantifies the impact of biomass burning aerosols on D-N temperature variations in this region but also provides valuable satellite-based insights that can help better constrain aerosol radiative effects in climate models.

Conflict of Interest

The authors declare no conflicts of interest relevant to this study.

Data Availability Statement

MERRA-2 data used in this study include monthly aerosol diagnostics (AOD, BC AOD, OC AOD, and sulfate AOD), meteorological temperature fields and carbon monoxide (CO) mixing ratios, all obtained from the NASA Goddard Earth Sciences Data and Information Services Center (Global Modeling and Assimilation Office [GMAO], 2015a, 2015b, 2015c). AIRS Level 3 monthly daytime and nighttime temperature data were also accessed from the NASA Goddard Earth Sciences Data and Information Services Center (AIRS Project, 2019). MODIS Aqua Aerosol Optical Depth (AOD) data were acquired from the NASA MODIS data repository (Levy et al., 2013b), available at https://modis.gsfc.nasa.gov/data/dataprod/mod08.php. MOPITT CO data were obtained from the NASA Atmospheric Science Data Center (Deeter, Edwards, Francis, Gille, Martínez-Alonso, et al., 2019). Principal component analysis (PCA) was performed using the sklearn.decomposition module. The PCA module in the scikit-learn Python library (Pedregosa et al., 2011) is available at https://scikit-learn.org/stable/. All data sets and software are publicly available through the repositories, and sources are cited in the References section.

References

Acevedo, O. C., & Fitzjarrald, D. R. (2001). The early evening surface-layer transition: Temporal and spatial variability. *Journal of the Atmospheric Sciences*, 58(17), 2650–2667. https://doi.org/10.1175/1520-0469(2001)058<2650:TEESLT>2.0.CO;2

AIRS Project. (2019). Aqua/AIRS L3 monthly standard physical retrieval (AIRS-only) 1 degree × 1 degree, version 7.0 [Dataset]. *NASA GES DISC*. https://doi.org/10.5067/UBENJB9D3T2H

Aumann, H. H., Chahine, M. T., Gautier, C., Goldberg, M. D., Kalnay, E., McMillin, L. M., et al. (2003). AIRS/AMSU/HSB on the Aqua mission: Design, science objectives, data products, and processing systems. *IEEE Transactions on Geoscience and Remote Sensing*, 41(2), 253–264. https://doi.org/10.1109/TGRS.2002.808356

Badarinath, K. V. S., Latha, K. M., Chand, T. K., & Gupta, P. K. (2009). Impact of biomass burning on aerosol properties over tropical wet evergreen forests of Arunachal Pradesh, India. *Atmospheric Research*, 91(1), 87–93. https://doi.org/10.1016/j.atmosres.2008.03.023

Bharali, C., Nair, V. S., Chutia, L., & Babu, S. (2019). Modeling of the effects of wintertime aerosols on boundary layer properties over the indo Gangetic plain. *Journal of Geophysical Research: Atmospheres*, 124(7), 4141–4157. https://doi.org/10.1029/2018JD029758

Bisht, D. S., Dumka, U. C., Kaskaoutis, D. G., Pipal, A. S., Srivastava, A. K., Soni, V. K., et al. (2015). Carbonaceous aerosols and pollutants over Delhi urban environment: Temporal evolution, source apportionment and radiative forcing. *Science of the Total Environment*, 521–522, 431–445. https://doi.org/10.1016/j.scitotenv.2015.03.083

Borgohain, A., Gogoi, M., Barman, N., Kundu, A., Banik, T., Kundu, S. S., et al. (2023). Impact of biomass burning on black carbon and NO₂ over North Eastern region of India using multi-satellite observations. *Journal of the Indian Society of Remote Sensing*, 51(8), 1605–1617. https://doi.org/10.1007/s12524-023-01692-2

Bosilovich, M. G., Akella, S., Coy, L., Cullather, R., Draper, R. C., Gelaro, R., et al. (2015). *MERRA-2: Initial evaluation of the climate. Technical report series on global modeling and data assimilation*. NASA Tech. Rep. NASA/TM– 2015-104606, (Vol. 43). https://ntrs.nasa.gov/citations/20160005045

Buchard, V., Randles, C. A., Da Silva, A. M., Darmenov, A., Colarco, P. R., Govindaraju, R., et al. (2017). The MERRA-2 aerosol reanalysis, 1980 onward. Part II: Evaluation and case studies. *Journal of Climate*, 30(17), 6851–6872. https://doi.org/10.1175/JCLI-D-16-0613.1

Buchholz, R. R., Deeter, M. N., Worden, H. M., Gille, J., Edwards, D. P., Hannigan, J. W., et al. (2017). Validation of MOPITT carbon monoxide using ground-based Fourier transform infrared spectrometer data from NDACC. *Atmospheric Measurement Techniques*, 10(5), 1927–1956. https://doi.org/10.5194/amt-10-1927-2017

Chahine, M. T., Pagano, T. S., Aumann, H. H., Atlas, R., Barnet, C., Blaisdell, J., et al. (2006). AIRS: Improving weather forecasting and providing new data on greenhouse gases. *Bulletin of the American Meteorological Society*, 87(7), 911–926. https://doi.org/10.1175/BAMS-87-7-911

Dai, A., Trenberth, K. E., & Karl, T. R. (1999). Effects of clouds, soil moisture, precipitation, and water vapor on diurnal temperature range. *Journal of Climate*, 12(8), 2451–2473. https://doi.org/10.1175/1520-0442(1999)012<2451:EOCSMP>2.0.CO;2

Dave, P., Bhushan, M., & Venkataraman, C. (2020). Absorbing aerosol influence on temperature maxima: An observation based study over India. *Atmospheric Environment*, 223, 117237. https://doi.org/10.1016/j.atmosenv.2019.117237

David, L. M., Ravishankara, A. R., Kodros, J. K., Venkataraman, C., Sadavarte, P., Pierce, J. R., et al. (2018). Aerosol optical depth over India. *Journal of Geophysical Research: Atmospheres*, 123(7), 3688–3703. https://doi.org/10.1002/2017JD027719

Davidi, A., Koren, I., & Remer, L. (2009). Direct measurements of the effect of biomass burning over the Amazon on the atmospheric temperature profile. *Atmospheric Chemistry and Physics*, 9(21), 8211–8221. https://doi.org/10.5194/acp-9-8211-2009

Davidi, A., Kostinski, A. B., Koren, I., & Lehahn, Y. (2012). Observational bounds on atmospheric heating by aerosol absorption: Radiative signature of transatlantic dust. *Geophysical Research Letters*, *39*(4). https://doi.org/10.1029/2011GL050358

Deeter, M. N., Edwards, D. P., Francis, G. L., Gille, J. C., Martínez-Alonso, S., Worden, H. M., & Sweeney, C. (2019). MOPITT carbon monoxide (CO) profiles, version 8 (MOP03JM) [Dataset]. *NASA Atmospheric Science Data Center (ASDC)*. https://asdc.larc.nasa.gov/project/MOPITT/MOP03JM_8

Deeter, M. N., Edwards, D. P., Francis, G. L., Gille, J. C., Mao, D., Martínez-Alonso, S., et al. (2019). Radiance-based retrieval bias mitigation for the MOPITT instrument: The version 8 product. *Atmospheric Measurement Techniques*, *12*(8), 4561–4580. https://doi.org/10.5194/amt-12-4561-2019

Deeter, M. N., Edwards, D. P., Francis, G. L., Gille, J. C., Martínez-Alonso, S., Worden, H. M., & Sweeney, C. (2017). A climate-scale satellite record for carbon monoxide: The MOPITT version 7 product. *Atmospheric Measurement Techniques*, *10*(7), 2533–2555. https://doi.org/10.5194/amt-10-2533-2017

Deeter, M. N., Emmons, L. K., Francis, G. L., Edwards, D. P., Gille, J. C., Warner, J. X., et al. (2003). Operational carbon monoxide retrieval algorithm and selected results for the MOPITT instrument. *Journal of Geophysical Research*, *108*(D14). https://doi.org/10.1029/2002JD003186

Diehl, T., Heil, A., Chin, M., Pan, X., Streets, D., Schultz, M., & Kinne, S. (2012). Anthropogenic, biomass burning, and volcanic emissions of black carbon, organic carbon, and SO_2 from 1980 to 2010 for hindcast model experiments. *Atmospheric Chemistry and Physics Discussions*, *12*, 824895–824954. https://doi.org/10.5194/acpd-12-24895-2012

Ding, F., Savtchenko, A., Hearty, T., Wei, J., Theobald, M., Vollmer, B., et al. (2020). Assessing the impacts of two averaging methods on AIRS level 3 monthly products and multiyear monthly means. *Journal of Atmospheric and Oceanic Technology*, *37*(6), 1027–1050. https://doi.org/10.1175/JTECH-D-19-0129.1

Drummond, J. (1993). *Measurements of pollution in the troposphere (MOPITT) instrument* (Vol. 1939, pp. 126–136). SPIE. https://doi.org/10.1117/12.152839

Drummond, J. R., Vaziri Zanjani, Z., Nichitiu, F., & Zou, J. (2022). A 20-year review of the performance and operation of the MOPITT instrument. *Advances in Space Research*, *70*(10), 3078–3091. https://doi.org/10.1016/j.asr.2022.09.010

Emmons, L. K., Edwards, D. P., Deeter, M. N., Gille, J. C., Campos, T., Nédélec, P., et al. (2009). Measurements of Pollution in the Troposphere (MOPITT) validation through 2006. *Atmospheric Chemistry and Physics*, *9*(5), 1795–1803. https://doi.org/10.5194/acp-9-1795-2009

Gelaro, R., McCarty, W., Suárez, M. J., Todling, R., Molod, A., Takacs, L., et al. (2017). The Modern-Era Retrospective Analysis for Research and Applications, version 2 (MERRA-2). *Journal of Climate*, *30*(14), 5419–5454. https://doi.org/10.1175/JCLI-D-16-0758.1

Girach, I. A., & Nair, P. R. (2014). Carbon monoxide over Indian region as observed by MOPITT. *Atmospheric Environment*, *99*, 599–609. https://doi.org/10.1016/j.atmosenv.2014.10.019

Global Modeling and Assimilation Office (GMAO). (2015a). MERRA-2 tavgM_2d_aer_Nx: 2D, monthly mean, time-averaged, single-level, assimilation, aerosol diagnostics V5.12.4 [Dataset]. *NASA Goddard Earth Sciences Data and Information Services Center (GES DISC)*. https://doi.org/10.5067/FH9A0MLJPC7N

Global Modeling and Assimilation Office (GMAO). (2015b). MERRA-2 inst3_3d_asm_Np: 3D, 3-Hourly, instantaneous, pressure-level, assimilation, assimilated meteorological fields V5.12.4 [Dataset]. *NASA Goddard Earth Sciences Data and Information Services Center (GES DISC)*. https://doi.org/10.5067/QBZ6MG944HW0

Global Modeling and Assimilation Office (GMAO). (2015c). MERRA-2 inst3_3d_chm_Nv: 3D, 3-Hourly, instantaneous, model-level, assimilation, carbon monoxide and ozone mixing ratio V5.12.4 [Dataset]. *NASA Goddard Earth Sciences Data and Information Services Center (GES DISC)*. https://doi.org/10.5067/HO9OVZWF3KW2

Gogoi, M. M., Babu, S. S., Moorthy, K. K., Bhuyan, P. K., Pathak, B., Subba, T., et al. (2017). Radiative effects of absorbing aerosols over northeastern India: Observations and model simulations. *Journal of Geophysical Research: Atmospheres*, *122*(2), 1132–1157. https://doi.org/10.1002/2016JD025592

Gupta, P., Remer, L. A., Levy, R. C., & Mattoo, S. (2018). Validation of MODIS 3 km land aerosol optical depth from NASA's EOS Terra and Aqua missions. *Atmospheric Measurement Techniques*, *11*(5), 3145–3159. https://doi.org/10.5194/amt-11-3145-2018

Hotelling, H. (1933). Analysis of a complex of statistical variables into principal components. *Journal of Educational Psychology*, *24*(6), 498–520. https://doi.org/10.1037/h0071325

Jethva, H., Torres, O., Field, R. D., Lyapustin, A., Gautam, R., & Kayetha, V. (2019). Connecting crop productivity, residue fires, and air quality over Northern India. *Scientific Reports*, *9*(1), 16594. https://doi.org/10.1038/s41598-019-52799-x

Jolliffe, I. T. (2002). *Principal component analysis* (2nd ed.), Springer. https://doi.org/10.1007/b98835

Kant, S., Sarangi, C., & Wilcox, E. M. (2023). Aerosol processes perturb cloud trends over Bay of Bengal: Observational evidence. *npj Climate and Atmospheric Science*, *6*(1), 132. https://doi.org/10.1038/s41612-023-00443-x

Khoir, A. N. U., Ooi, M. C. G., Juneng, L., Ramadhan, M. A. I., Virgianto, R. H., & Tangang, F. (2022). Spatio-temporal analysis of aerosol optical depth using rotated empirical orthogonal function over the Maritime continent from 2001 to 2020. *Atmospheric Environment*, *290*, 119356. https://doi.org/10.1016/j.atmosenv.2022.119356

Kumar, S., Kumar, S., Kaskaoutis, D. G., Singh, R. P., Singh, R. K., Mishra, A. K., et al. (2015). Meteorological, atmospheric and climatic perturbations during major dust storms over Indo-Gangetic Basin. *Aeolian Research*, *17*, 15–31. https://doi.org/10.1016/j.aeolia.2015.01.006

Kuttippurath, J., & Raj, S. (2021). Two decades of aerosol observations by AATSR, MISR, MODIS and MERRA-2 over India and Indian Ocean. *Remote Sensing of Environment*, *257*, 112363. https://doi.org/10.1016/j.rse.2021.112363

Levy, R. C., Mattoo, S., Munchak, L. A., Remer, L. A., Sayer, A. M., Patadia, F., & Hsu, N. C. (2013a). The collection 6 MODIS aerosol products over land and ocean. *Atmospheric Measurement Techniques*, *6*(11), 2989–3034. https://doi.org/10.5194/amt-6-2989-2013

Levy, R. C., Mattoo, S., Munchak, L. A., Remer, L. A., Sayer, A. M., Patadia, F., & Hsu, N. C. (2013b). MODIS aqua aerosol optical depth product (MOD08_M3) [Dataset]. *NASA MODIS Data Repository*. https://modis.gsfc.nasa.gov/data/dataprod/mod08.php

Levy, R. C., Remer, L. A., & Dubovik, O. (2007). Global aerosol optical properties and application to Moderate resolution imaging spectroradiometer aerosol retrieval over land. *Journal of Geophysical Research*, *112*(D13). https://doi.org/10.1029/2006JD007815

Li, J., Carlson, B. E., & Lacis, A. A. (2013). Application of spectral analysis techniques in the intercomparison of aerosol data: 1. An EOF approach to analyze the spatial-temporal variability of aerosol optical depth using multiple remote sensing data sets. *Journal of Geophysical Research: Atmospheres*, *118*(15), 8640–8648. https://doi.org/10.1002/jgrd.50686

Li, J., Carlson, B. E., & Lacis, A. A. (2014). Application of spectral analysis techniques in the intercomparison of aerosol data: Part III. Using combined PCA to compare spatiotemporal variability of MODIS, MISR, and OMI aerosol optical depth. *Journal of Geophysical Research: Atmospheres*, *119*(7), 4017–4042. https://doi.org/10.1002/2013JD020538

Li, J., Carlson, B. E., Yung, Y. L., Lv, D., Hansen, J., Penner, J. E., et al. (2022). Scattering and absorbing aerosols in the climate system. *Nature Reviews Earth & Environment*, *3*(6), 363–379. https://doi.org/10.1038/s43017-022-00296-7

Lu, Z., Wang, J., Chen, X., Zeng, J., Wang, Y., Xu, X., et al. (2023). First mapping of monthly and diurnal climatology of Saharan dust layer height over the Atlantic Ocean from EPIC/DSCOVR in deep space. *Geophysical Research Letters*, *50*(5), e2022GL102552. https://doi.org/10.1029/2022GL102552

Ma, Y., Li, Z., Li, Z., Xie, Y., Fu, Q., Li, D., et al. (2016). Validation of MODIS aerosol optical depth retrieval over Mountains in central China based on a sun-sky radiometer site of SONET. *Remote Sensing*, *8*(2), 111. https://doi.org/10.3390/rs8020111

McCarty, W., Coy, L., Gelaro, R., Huang, A., Merkova, D., Smith, E. B., et al. (2016). *MERRA-2 input observations: Summary and initial assessment. Technical report series on global modeling and data assimilation*. NASA Tech. Rep. NASA/TM—2016–104606, (Vol. 46) https://gmao.gsfc.nasa.gov/pubs/docs/McCarty885.pdf

Mondal, A., Sah, N., Sharma, A., Venkataraman, C., & Patil, N. (2021). Absorbing aerosols and high-temperature extremes in India: A general circulation modelling study. *International Journal of Climatology's*, *41*(Suppl. 1), E1498–E1517. https://doi.org/10.1002/joc.6783

Myhre, G., Samset, B. H., Schulz, M., Balkanski, Y., Bauer, S., Berntsen, T. K., et al. (2013). Radiative forcing of the direct aerosol effect from AeroCom phase II simulations. *Atmospheric Chemistry and Physics*, *13*(4), 1853–1877. https://doi.org/10.5194/acp-13-1853-2013

Pan, X., Chin, M., Gautam, R., Bian, H., Kim, D., Colarco, P. R., et al. (2015). A multi-model evaluation of aerosols over South Asia: Common problems and possible causes. *Atmospheric Chemistry and Physics*, *15*(10), 5903–5928. https://doi.org/10.5194/acp-15-5903-2015

Pandey, S. K., & Vinoj, V. (2021). Surprising changes in aerosol loading over India amid COVID-19 lockdown. *Aerosol and Air Quality Research*, *21*(3), 200466. https://doi.org/10.4209/aaqr.2020.07.0466

Payra, S., Sharma, A., Mishra, M. K., & Verma, S. (2023). Performance evaluation of MODIS and VIIRS satellite AOD products over the Indian subcontinent. *Frontiers in Environmental Science*, *11*, 1158641. https://doi.org/10.3389/fenvs.2023.1158641

Pearson, K. (1901). Principal components analysis. *The London, Edinburgh, and Dublin Philosophical Magazine and Journal of Science*, *6*, 559.

Pedregosa, F., Varoquaux, G., Gramfort, A., Michel, V., Thirion, B., Grisel, O., et al. (2011). Scikit-learn, scikit-learn: Machine learning in python [Software]. *Journal of Machine Learning Research*, *12*, 2825–2830. https://scikit-learn.org/stable/

Platnick, S., King, M., Meyer, K., Wind, G., Amarasinghe, N., Marchant, B., et al. (2015). *MODIS atmosphere L3 monthly product. NASA MODIS adaptive processing system* (Vol. 20). Goddard Space Flight Center.

Ramachandran, S., & Kedia, S. (2010). Black carbon aerosols over an urban region: Radiative forcing and climate impact. *Journal of Geophysical Research*, *115*(D10), D10202. https://doi.org/10.1029/2009JD013560

Ramachandran, S., Rupakheti, M., Cherian, R., & Lawrence, M. G. (2023). Aerosols heat up the Himalayan climate. *Science of the Total Environment*, *894*, 164733. https://doi.org/10.1016/j.scitotenv.2023.164733

Ramachandran, S., Rupakheti, M., & Lawrence, M. G. (2020). Black carbon dominates the aerosol absorption over the Indo-Gangetic plain and the Himalayan foothills. *Environment International*, *142*, 105814. https://doi.org/10.1016/j.envint.2020.105814

Ramanathan, V., Ramana, M. V., Roberts, G., Kim, D., Corrigan, C., Chung, C., & Winker, D. (2007). Warming trends in Asia amplified by brown cloud solar absorption. *Nature*, *448*(7153), 575–578. https://doi.org/10.1038/nature06019

Randles, C. A., da Silva, A. M., Buchard, V., Colarco, P. R., Darmenov, A., Govindaraju, R., et al. (2017). The MERRA-2 aerosol reanalysis, 1980 onward. Part I: System description and data assimilation evaluation. *Journal of Climate*, *30*(17), 6823–6850. https://doi.org/10.1175/JCLI-D-16-0609.1

Remer, L. A., Kaufman, Y. J., Tanré, D., Mattoo, S., Chu, D. A., Martins, J. V., et al. (2005). The MODIS aerosol algorithm, products, and validation. *Journal of the Atmospheric Sciences*, *62*(4), 947–973. https://doi.org/10.1175/JAS3385.1

Rienecker, M. M., Suarez, M. J., Todling, R., Bacmeister, J., Takacs, L., Liu, H.-C., et al. (2008). *The GEOS-5 data assimilation system—documentation of versions 5.0.1, 5.1.0, and 5.2.0. technical report series on global modeling and data assimilation*. NASA Tech. Rep. NASA/TM-2008-104606, (Vol. 27).

Ruzmaikin, A., Aumann, H. H., Lee, J., & Susskind, J. (2017). Diurnal cycle variability of surface temperature inferred from AIRS data. *Journal of Geophysical Research: Atmospheres*, *122*(20), 10928–10938. https://doi.org/10.1002/2016JD026265

Safai, P. D., Raju, M. P., Maheshkumar, R. S., Kulkarni, J. R., Rao, P. S. P., & Devara, P. C. S. (2012). Vertical profiles of Black carbon aerosols over the urban locations in South India. *Science of the Total Environment*, *431*, 323–331. https://doi.org/10.1016/j.scitotenv.2012.05.058

Samset, B. H., Stjern, C. W., Andrews, E., Kahn, R. A., Myhre, G., Schulz, M., & Schuster, G. L. (2018). Aerosol absorption: Progress towards global and regional constraints. *Current Climate Change Reports*, *4*(2), 65–83. https://doi.org/10.1007/s40641-018-0091-4

Sarkar, S., Chauhan, A., Kumar, R., & Singh, R. P. (2019). Impact of deadly dust storms (May 2018) on air quality, meteorological, and atmospheric parameters over the Northern parts of India. *GeoHealth*, *3*(3), 67–80. https://doi.org/10.1029/2018gh000170

Shen, X., Liu, B., & Lu, X. (2017). Effects of land use/land cover on diurnal temperature range in the temperate grassland region of China. *Science of the Total Environment*, *575*, 1211–1218. https://doi.org/10.1016/j.scitotenv.2016.09.187

Song, J., Wang, J., Xia, X., Lin, R., Wang, Y., Zhou, M., & Fu, D. (2021). Characterization of urban heat Islands using city lights: Insights from MODIS and VIIRS DNB observations. *Remote Sensing*, *13*(16), 3180. https://doi.org/10.3390/rs13163180

Stjern, C. W., Samset, B. H., Boucher, O., Iversen, T., Lamarque, J. F., Myhre, G., et al. (2020). How aerosols and greenhouse gases influence the diurnal temperature range. *Atmospheric Chemistry and Physics*, *20*(21), 13467–13480. https://doi.org/10.5194/acp-20-13467-2020

Strode, S. A., & Pawson, S. (2013). Detection of carbon monoxide trends in the presence of interannual variability. *Journal of Geophysical Research: Atmospheres*, *118*(21), 12257–212273. https://doi.org/10.1002/2013JD020258

Tian, B., Manning, E., Roman, J., Thrastarson, H., Fetzer, E., & Monarrez, R. (2020). *AIRS version 7 level 3 product user guide, version 1.1*, Tech. Rep., Jet Propulsion Laboratory. California Institute of Technology.

Wang, J., & Christopher, S. A. (2006). Mesoscale modeling of Central American smoke transport to the United States: 2. Smoke radiative impact on regional surface energy budget and boundary layer evolution. *Journal of Geophysical Research*, *111*(D14). https://doi.org/10.1029/2005JD006720

Wei, J., Peng, Y., Guo, J., & Sun, L. (2019). Performance of MODIS collection 6.1 level 3 aerosol products in spatial-temporal variations over land. *Atmospheric Environment*, *206*, 30–44. https://doi.org/10.1016/j.atmosenv.2019.03.001

Wilcox, E. M. (2010). Stratocumulus cloud thickening beneath layers of absorbing smoke aerosol. *Atmospheric Chemistry and Physics*, *10*(23), 11769–11777. https://doi.org/10.5194/acp-10-11769-2010

Wilcox, E. M., Thomas, R. M., Praveen, P. S., Pistone, K., Bender, F. A., & Ramanathan, V. (2016). Black carbon solar absorption suppresses turbulence in the atmospheric boundary layer. *Proceedings of the National Academy of Sciences*, *113*(42), 11794–11799. https://doi.org/10.1073/pnas.1525746113

Zhang, L., Ding, M., Zheng, X., Chen, J., Guo, J., & Bian, L. (2023). Assessment of AIRS version 7 temperature profiles and low-level inversions with GRUAN radiosonde observations in the Arctic. *Remote Sensing*, *15*(5), 1270. https://doi.org/10.3390/rs15051270

Zhang, X., Liu, J., Han, H., Zhang, Y., Jiang, Z., Wang, H., et al. (2020). Satellite-observed variations and trends in carbon monoxide over Asia and their sensitivities to biomass burning. *Remote Sensing*, *12*(5), 830. https://doi.org/10.3390/rs12050830